Mediated Charge Transfer at Nanoelectrodes: a New Approach to Electrochemical Reactivity Mapping and Nanosensing

Koushik Barman,[†] Xiang Wang,[†,§] Rui Jia,[†,§] and Michael V. Mirkin[†,§,*]

† Department of Chemistry and Biochemistry, Queens College-CUNY, Flushing, NY 11367, USA.

§ The Graduate Center of CUNY, New York, NY 10016.

Supporting Information Placeholder

ABSTRACT: Scanning electrochemical microscopy (SECM) is a powerful tool for mapping surface reactivity. Electrochemical mapping of electrocatalytic processes at the nanoscale is, however, challenging because the surface of a nanoelectrode tip is easily fouled by impurities and/or deactivated by products and intermediates of inner-sphere surface reactions. To overcome this difficulty, we introduce a new type of SECM nanotips based on bimolecular electron transfer between the dissolved electroactive species and a redox mediator attached to the surface of a carbon nanoelectrode. Tris(2,2'-bipyridine)ruthenium complex, $Ru(bpy)_3$, that undergoes reversible oxidation/reduction reactions at both positive and negative potentials was used to prepare the SECM nanoprobes for mapping a wide range of electrocatalytic processes through oxidation of H_2, reduction of O_2 and both oxidation and reduction of H_2O_2 at the tip. In addition to high-resolution reactivity mapping and localized kinetic measurements, chemically modified nanoelectrodes can serve as nanosensors for a number of important analytes such as reactive oxygen and nitrogen species and neurotransmitters.

Significant recent advances in nanoscale electrochemical mapping of heterogeneous surface reactivity have been made by using nanometer-sized metal electrodes as scanning electrochemical microscopy (SECM) tips.[1-6] Metal nanoelectrodes are most suitable for measuring currents produced by outer-sphere electron transfer (ET) reactions that have often been the subject of earlier SECM studies.[7,8] By contrast, electrocatalytic, electrosynthetic, and bioelectrochemical systems typically involve inner-sphere processes that can be probed in the substrate generation/tip collection (SG/TC) mode of SECM, in which the tip collects the redox species generated at the substrate surface.[2,4,5] Unlike outer-sphere ET processes, reactants, products, and intermediates of heterogeneous inner-sphere reactions (oxygen, reactive oxygen/nitrogen species, catecholamines) typically passivate the nanoelectrode surface. Inner-sphere reactions are also sensitive to adsorbed impurities that block active atoms needed to carry out such a reaction.[9-11] The smaller the tip electrode, the stronger the effects of its surface deactivation or contamination, and the harder to measure signals produced by electrocatalytic processes.

Herein we introduce chemically modified nanoelectrodes for mediated oxidation/reduction of electroactive species that deactivate the surface of bare metal nanotips. A reversible redox mediator is attached to the surface of a carbon nanoelectrode (CNE) produced by chemical vapor deposition of carbon into a quartz capillary.[12,13] Although chemically modified nanosensors have previously been fabricated,[14-17] nanoelectrodes and SECM nanotips based on mediated ET have not yet been reported.

We previously used Pt nanotips for mapping of MoS_2 [5] and MXenes[18] activity toward the hydrogen evolution reaction (HER). In those experiments, ferrocenemethanol (Fc) mediator was added to the solution to image surface topography and locate a microscopic domain of interest for reactivity mapping. Surprisingly, HER mapping could not be done without Fc mediator because the tip current (i_T) produced by hydrogen oxidation reaction (HOR) at the tip decreased precipitously with time, precluding substrate surface imaging. In Fig. S1, a nanotip with the radius, $a \approx 50$ nm was positioned at a micrometer distance from the macroscopic Pt substrate generating H_2 in 10 mM $HClO_4$ solution. The i_T decreased rapidly with no Fc present (red curve in Fig. S1), but no similar decay was observed after adding Fc to the solution (black curve). The essentially time-independent $i_T = 60$ pA could not be due to Fc oxidation at the tip surface that could only produce <10 pA diffusion-limited current. Moreover, the black curve in Fig. S1 was obtained with a carbon (rather than Pt) tip at whose surface the direct oxidation of hydrogen is immeasurably slow at the applied potential value (0 V vs. Hg/Hg_2SO_4 reference). This data suggests that the tip current measured in the presence of Fc is produced by the mediated H_2 oxidation:

$$Fc - e^- = Fc^+ \quad \text{(nanotip)} \qquad (1)$$

$$H_2 + 2Fc^+ = 2H^+ + 2Fc \quad \text{(tip/substrate gap)} \qquad (2)$$

Unlike the inner-sphere, surface-dependent HOR at a Pt tip, the oxidation of Fc (reaction 1) is a rapid outer-sphere ET process[7] whose rate is less sensitive to the surface contamination and passivation.[9,11] Reaction 2 is fast because of the sufficiently positive standard potential of Fc^+/Fc couple (~0.15 V vs. Ag/AgCl).

To avoid possible interference of dissolved mediator species with the system under study, we immobilized electroactive moieties on the nanotip surface. Although ferrocene moieties can be attached to a CNE surface and used to mediate ET reactions (Fig. S2), because of space limitations our discussion will focus on $Ru(bpy)_3$-modified carbon nanoelectrodes that showed the best electrochemical responses. Modified nanoelectrodes were prepared by applying a sufficiently positive potential to a CNE in solution containing $Ru(bpy)_3^{2+}$ (Supplementary materials and methods). Similar to the literature protocol used for glassy carbon electrodes,[19] this procedure requires no additional chemical agents and results in direct attachment of $Ru(bpy)_3$ to the carbon surface with no spacer.

$Ru(bpy)_3$-modified CNEs yielded well-shaped cyclic voltammograms (CVs; Fig. 1A) with the peak current directly proportional to the potential sweep rate (v; the inset) and excellent response stability (Fig. S3) over a time period of several days. The integration of the current under either the anodic or cathodic peak yields the charge corresponding to the total amount of $Ru(bpy)_3$ bound to the CNE surface. Very similar charge values (52.5 ± 3 pC) corresponding to 0.54 ± 0.03 fmol of $Ru(bpy)_3$ have been obtained from five anodic and cathodic peaks in Fig. 1A.

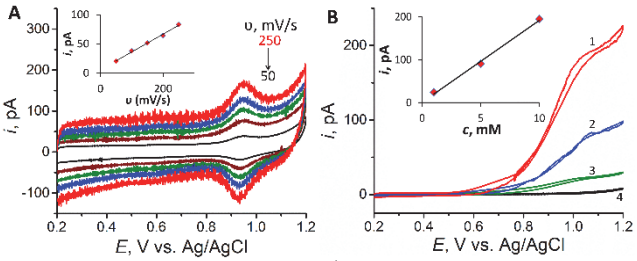

Figure 1. Voltammograms of $Ru(bpy)_3^{3/2+}$ couple (A) and of mediated H_2O_2 oxidation (B) at the same $Ru(bpy)_3$-modified 50-nm-radius CNE. Solution contained 0.1 M KNO_3. (B) $c_{H_2O_2}$, mM = 10 (1), 5 (2), and 1 (3). Curve 4 is the voltammogram of 10 mM H_2O_2 at a bare CNE. v = 3 mV/s. Insets: (A) scan rate dependence of the anodic peak current; (B) dependence of the plateau current on $c_{H_2O_2}$ obtained from curves 1-3.

The same $Ru(bpy)_3$-modified CNE was used to measure the mediated oxidation of hydrogen peroxide (Fig. 1B). The ability to monitor H_2O_2 at the nanoscale is important for mapping of electrochemical reactivity of catalysts and biomedical research.[20-24] The oxidation of H_2O_2 rapidly passivates the surface of a Pt nanotip, so that platinized nanoelectrodes with a much larger true surface area had to be used to measure H_2O_2 and other reactive oxygen and nitrogen species in biological cells.[15,25] However, such nanoelectrodes are not suitable for surface reactivity mapping. Unlike a bare carbon nanoelectrode (curve 4 in Fig. 1B), a $Ru(bpy)_3$-modified CNE produced well-defined steady-state voltammograms of H_2O_2 oxidation (curves 1-3) with the limiting current directly proportional to its bulk concentration (the inset).

The plateau current can be either diffusion limited or kinetic, i.e., controlled by the rate of reaction between the surface-bound mediator (e.g., $Ru(bpy)_3^{3+}$) and the redox species dissolved in solution (e.g., H_2O_2; reaction S2 in Supporting Information). The diffusion-limited current is

$$i_d = 4xnFac_{H_2O_2}D_{H_2O_2} \quad (1)$$

where n is the number of transferred electrons (i.e. 2 for H_2O_2), F is Faraday constant, $D_{H_2O_2} = 1.4 \times 10^{-5}$ cm^2/s [26] and $c_{H_2O_2}$ are the diffusion coefficient and concentration of H_2O_2 in the aqueous solution, respectively. The factor x is a function of RG (i.e., the ratio of glass radius to that of the conductive tip); x = 1.16 corresponds to RG = 1.5 typical of thick-wall quartz pipettes used in this study.[27] The limiting currents in Fig. 1B are less than one third of the i_d values expected from Eq. (1), pointing to the finite kinetics of the mediated charge-transfer process. The kinetic limiting current is:

$$i_k = AnFkc_{H_2O_2}[Ru(bpy)_3] \quad (2)$$

where A is the surface area of $Ru(bpy)_3$-modified CNE, k is the rate constant of reaction (S2) and $[Ru(bpy)_3]$ is the surface concentration of the mediator. Using the amount of charge corresponding to the $Ru(bpy)_3^{2+}$ oxidation ($AF[Ru(bpy)_3] = 52.5$ pC from Fig. 1A), the apparent rate constant value, k = (3.0±0.5) $\times 10^5$ $M^{-1}s^{-1}$ was extracted from H_2O_2 voltammograms in Fig. 1B (Supporting Information). As expected, the peak potentials in Fig. 1A (~0.93 V) are very close to the half-wave potential of the H_2O_2 oxidation in Fig. 1B.

Both diffusion-limited and kinetic currents are directly proportional to $c_{H_2O_2}$, and so each of them can be used for measuring the H_2O_2 flux and mapping surface reactivity by SECM. The currents of H_2O_2 oxidation (Fig. S4A) and HOR (Fig. S4B) at $Ru(bpy)_3$-modified CNEs are very stable because these mediated processes are not sensitive to surface contamination/deactivation (see above). The i_T stability enables feedback mode (Fig. 2A) and SG/TC mode (Fig. 2B) imaging with $Ru(bpy)_3$-modified CNEs tips. In Fig. 2A, H_2O_2 was oxidized at the tip and regenerated via the oxygen reduction (ORR) at the Au nanoparticle (NP) attached to the HOPG surface (Scheme S1a). H_2O_2 is known to be a major product of the ORR at Au NPs.[28] A feedback topographic image of an AFM standard (Fig. S9) shows that the SECM with a $Ru(bpy)_3$-modified CNE tip faithfully reproduces the shape of a sample.

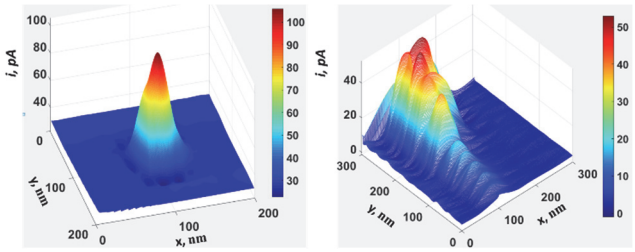

Figure 2. Feedback mode (A) and SG/TC mode (B) images of 100 nm diameter Au NP on the HOPG/aminophenyl surface obtained with ~100 nm $Ru(bpy)_3$-modified CNEs. Solution contained (A) 10 mM H_2O_2 in 0.1 M phosphate buffer (PB; pH7.2) and (B) 0. 1 M PB. The substrate potential, E_S = -0.8 V (A) and -0.9 vs. Ag/AgCl (B). The tip potential, E_T = 1.3 V vs Ag/AgCl.

In addition to $Ru(bpy)_3^{3/2+}$ peaks (Fig. 1A), CVs of $Ru(bpy)_3$ complex obtained in organic solvents over a wide potential range show several pairs of peaks of ET reactions occurring at more negative potentials.[29] In voltammograms obtained at $Ru(bpy)_3$-modified CNEs in aqueous solutions such peaks are less prominent, like those occurring at about -0.6 V and +0.3 V (labeled with the blue and green circles in Fig. 3A). Importantly, the ET process occurring at -0.6 V efficiently mediates inner-sphere reduction reactions, including the reduction of H_2O_2 (Figs. 3B and 3C) and ORR (Fig. 3D). The half-wave potential of the well-defined H_2O_2 reduction voltammogram (—0.6 V; curve 2 in Fig. 3B) is very close to the mid-peak potential marked the blue circle in Fig. 3A. By contrast, the voltammogram of 10 mM H_2O_2 obtained at a bare CNE under the same experimental conditions (curve 1 in Fig. 3B) is essentially flat and featureless. The plateau current of the mediated H_2O_2 reduction is directly proportional to $c_{H_2O_2}$ (the inset in Fig. 3C). The limiting current values are similar to those of H_2O_2 oxidation (Fig. 1B), indicating that the rate of the $Ru(bpy)_3$ mediated reduction is also kinetically controlled. The linear concentration dependence of i_T and its high temporal stability (Fig. S5A) suggest that the H_2O_2 reduction at $Ru(bpy)_3$-modified tips is suitable for SECM imaging and nanosensing applications.

The half-wave potential of the $Ru(bpy)_3$-mediated ORR (about —0.6 V; Fig. 3D) is very similar to that of the H_2O_2 reduction (Fig. 3C) because both processes are mediated by the same ET at the CNP surface (labeled with the blue circle in Fig. 3A). The ORR plateau current is directly proportional to the bulk concentration of O2 (the inset in Fig 3D) and stable on the time scale of minutes (Fig. S5B). By contrast, ORR passivates the surface of metal nanoelectrodes hindering the SECM imaging.

The ORR current was used to obtain an approach curve and position a $Ru(bpy)_3$-modified CNE tip near the HOPG surface using the SECM negative feedback in PB solution with no added redox species (Fig. S6 and Scheme S1B). Then, the tip potential was

switched to a positive value (E_T = 1.3 V vs. Ag/AgCl) to oxidize H_2O_2 generated at the Au NP surface. The tip was scanned over the Au NP attached to the HOPG/aminophenyl surface to obtain a SG/TC map of the H_2O_2 flux (Fig. 2B and Scheme S1C). The lateral resolution of SG/TC maps is affected by the diffusion broadening, and so the particle in Fig. 2B appears to be much larger than a feedback-mode topographic image of a similar Au NP (Fig. 2A).

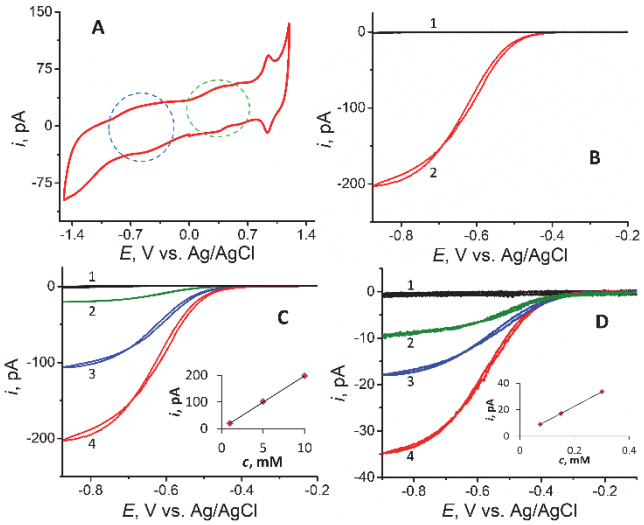

Figure 3. CV of $Ru(bpy)_3$ attached to a CNE surface (A) and voltammograms of $Ru(bpy)_3$-mediated H_2O_2 reduction (B,C) and ORR (D) at a modified CNE. $a \approx 50$ nm. υ, mV/s = 100 (A) and 3 (B-D). Electrolyte solution was: (A) Ar purged 0.1 M KNO_3; (B) 10 mM H_2O_2 in 0.1 M PBS; and 0.1 M PBS containing (C) 0 (1), 1 (2), 5 (3) and 10 (4) mM H_2O_2; and (D) 0 (Ar purged; 1), 0.075 (2), 0.15 (3), and 0.3 (4) mM O_2. Curve 1 in panel B was recorded at a bare CNE.

Mediated ET at nanoelectrodes can significantly improve sensitivity of electrochemical nanosensing. Amperometric sensors for many important analytes, such as reactive oxygen and nitrogen species and catecholamines, are based on inner-sphere ET processes that require a sufficiently large electrode surface area to obtain a well-defined and stable response. For instance, no analytically useful response to dopamine can be recorded at a flat disk-shaped nanoelectrode (curves 1 in Figs. 4A and 4B), and carbon nanofibers[30,31] and nanopipettes[32,33] with a relatively large surface area have been used for dopamine analysis in single cells and vesicles. Curves 2 in Figs. 4A and 4B show voltammograms of 100 µM (A) and 10 µM (B) dopamine at a 50-nm-radius $Ru(bpy)_3$-modified CNE with plateau currents close to the diffusion limit given by Eq. (1) that would not be possible to measure with a bare

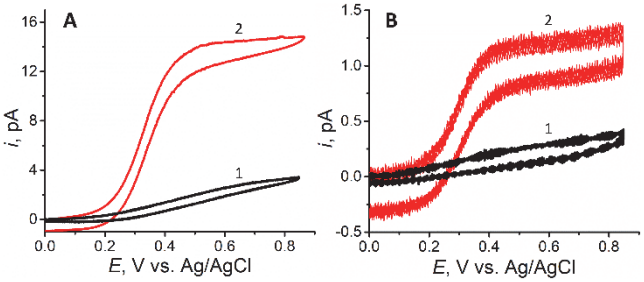

Figure 4. Voltammograms of dopamine at bare (1) and $Ru(bpy)_3$-modified (2) CNEs. $a \approx 50$ nm. υ = 10 mV/s. 0.1 M PBS contained (A) 100 µM and (B) 10 µM dopamine.

carbon nanodisk. The half-wave potential of the $Ru(bpy)_3$-mediated oxidation of dopamine (about 0.3 V) corresponds to the mid-peak potential for the ET at the modified CNE labeled with the green circle in Fig. 3A.

In conclusion, we demonstrated the possibility of direct attachment of an outer-sphere redox mediator to a carbon nanoelectrode surface to enable mediated oxidation/reduction of dissolved electroactive species. Using this approach, one can measure inner-sphere ET reactions at nanoelectrodes, which is essential for high-resolution electrochemical mapping of surface reactivity and amperometric nanosensing. Because carbon is catalytically inert, the rates of inner-sphere reactions on the CNE surface are negligibly slow, and the measured current was entirely due to the mediated ET process. A small RG (1.1-1.5) makes CNEs especially suitable as tips for surface reactivity mapping by SECM and intracellular measurements.[27]

$Ru(bpy)_3$ complex is exceptionally useful as a redox mediator for chemically modified nanoelectrodes. First, it can be attached directly to the carbon surface without using any additional chemical agents. Unlike self-assembled monolayers often employed for immobilizing redox moieties on surfaces, the $Ru(bpy)_3$ coating is robust and not affected by application of high positive or negative potentials to the modified nanoelectrode. The absence of a log-chain spacer and the fast self-exchange rate constant of $Ru(bpy)_3$ couple result in a fast mediated ET reaction between the modified CNE and dissolved redox species that produces a sufficiently high faradaic current at a nanoelectrode. Moreover, the same $Ru(bpy)_3$-modified CNE can be used to measure a broad range of oxidation and reduction processes, including ORR, HOR, oxidation and reduction of H_2O_2, and oxidation of dopamine. Other redox mediators with fast self-exchange rate constants and different standard potentials (e.g., tetrathiafulvalene or tetracyanoquinodimethane[34]) can be immobilized on the carbon tip surface to attain selective detection of various dissolved electroactive molecules.

ASSOCIATED CONTENT

Supporting Information. Experimental details, protocols for immobilizing ferrocene and $Ru(bpy)_3^{2+}$ on CNEs, kinetic analysis of mediated ET at CNEs, additional current-time recordings, and TEM images of CNEs, including Figures S1 – S8 and Scheme 1. This material is available free of charge via the Internet at http://pubs.acs.org.

AUTHOR INFORMATION

Corresponding Author

* mmirkin@qc.cuny.edu;

Notes

The authors declare no competing financial interests.

ACKNOWLEDGMENT

The support of this work by the National Science Foundation (CHE-2102298) is gratefully acknowledged.

REFERENCES

(1) Amemiya, S., Nanoscale Scanning Electrochemical Microscopy. In *Electroanalytical Chemistry: A Series of Advances*, Bard, A. J.; Zoski, C. G., Eds. CRC press: 2015; Vol. 26, pp 1-72.

(2) Kim, J.; Renault, C.; Arroyo-Currás, N.; Nioradze, N.; Leonard, K. C.; Bard, A. J. Electrocatalytic Activity of Individual Pt Nanoparticles Studied by Nanoscale Scanning Electrochemical Microscopy. *J. Am. Chem. Soc.* **2016**, *138*, 8560-8568.

(3) Bentley, C. L.; Edmondson, J.; Meloni, G. N.; Perry, D.; Shkirskiy, V.; Unwin, P. R. Nanoscale Electrochemical Mapping. *Anal. Chem.* **2019**, *91*, 84−108.

(4) Sun, T.; Wang, D.; Mirkin, M. V.; Cheng, H.; Zheng, J.-C.; Richards, R. M.; Lin, F.; Xin, H. L. Direct High-Resolution Mapping of Electrocatalytic Activity of Semi-Two-Dimensional Catalysts with Single-Edge Sensitivity. *Proc. Natl. Acad. Sci. USA* **2019**, *116*, 11618-11623.
(5) Sun, T.; Zhang, H.; Wang, X.; Liu, J.; Xiao, C.; Nanayakkara, S. U.; Blackburn, J. L.; Mirkin, M. V.; Miller, E. M. Nanoscale Mapping of Hydrogen Evolution on Metallic and Semiconducting MoS_2 Nanosheets. *Nanoscale Horiz.* **2019**, *4*, 619 – 624.
(6) Wang, X.; Askarova, G.; Mirkin, M. V. Electrochemical Microscopy at the Nanoscale, in *Nanoscale Electrochemistry (*Wain, A., Dickinson, E., Eds*);* Elsevier Ltd., 2021, in press, ISBN: 9780128200551.
(7) Sun, P.; Mirkin, M. V. Kinetics of Rapid Electron Transfer Reactions at Nanoelectrodes. *Anal. Chem.* **2006**, *78*, 6526-6534.
(8) Kai, T.; Zoski, C.; Bard, A. J. Scanning Electrochemical Microscopy at the Nanometer Level. *Chem. Commun.* **2018**, *54*, 1934–1947.
(9) Bard, A. J. Inner-Sphere Heterogeneous Electrode Reactions. Electrocatalysis and Photocatalysis: The Challenge. *J. Am. Chem. Soc.* **2010**, *132*, 7559-7567.
(10) Lhenry, S.; Leroux, Y. R.; Hapiot, P. Use of Catechol As Selective Redox Mediator in Scanning Electrochemical Microscopy Investigations. *Anal. Chem.* **2012**, *84*, 7518–7524.
(11) Nioradze, N.; Chen, R.; Kurapati, N.; Khvataeva-Domanov, A.; Mabic, S.; Amemiya, S. Organic Contamination of Highly Oriented Pyrolytic Graphite as Studied by Scanning Electrochemical Microscopy. *Anal. Chem.* **2015**, *87*, 4836–4843.
(12) Singhal, R.; Bhattacharyya, S.; Orynbayeva, Z.; Vitol, E.; Friedman, G.; Gogotsi, Y. Small diameter carbon nanopipettes. *Nanotechnology* **2010,** *21*, 015304.
(13) Yu, Y.; Gao, Y.; Hu, K.; Blanchard, P.-Y.; Noël, J.-M.; Nareshkumar, T.; Phani, K. L.; Friedman, G.; Gogotsi, Y.; Mirkin, M. V. Electrochemistry and Electrocatalysis at Single Gold Nanoparticles Attached to Carbon Nanoelectrodes. *ChemElectroChem* **2015**, *2*, 58–63.
(14) Guo, J.; Ho, C.-N.; Sun, P. Electrochemical Studies of Chemically Modified Nanometer-Sized Electrodes. *Electroanalysis* **2011**, *23*, 481-486.
(15) Hu, K.; Gao, Y.; Wang, Y.; Yu, Y.; Zhao, X.; Rotenberg, S. A.; Gökmeşe, E.; Mirkin, M. V.; Friedman, G.; Gogotsi, Y. Platinized Carbon Nanoelectrodes as Potentiometric and Amperometric SECM Probes. *J. Solid State Electrochem.* **2013***, 17,* 2971–2977.
(16) Clausmeyer, J.; Actis, P.; López Córdoba, A.; Korchev, Y.; Schuhmann, W. Nanosensors for the detection of hydrogen peroxide. *Electrochem. Commun.* **2014**, *40*, 28–30.
(17) Michalak, M.; Kurel, M.; Jedraszko, J.; Toczydlowska, Diana; Wittstock, G.; Opallo, M.; Nogala, W. Voltammetric pH Nanosensor. *Anal. Chem.* **2015**, *87*, 11641–11645.
(18) Djire, A.; Wang, X.; Xiao, C.; Nwamba, O. C.; Mirkin, M. V.; Neale, N. R. Basal Plane Hydrogen Evolution Activity from Mixed Metal Nitride MXenes Measured by Scanning Electrochemical Microscopy. *Adv. Funct. Mater.* **2020**, *30*, 202001136.
(19) Premkumar, J.; Khoo, S. B. Immobilization of ruthenium(II)bipyridyl complex at highly oxidized glassy carbon electrodes. *Electrochem. Commun.* **2004**, *6*, 984–989.
(20) Chen, W.; Cai, S.; Ren, Q.-Q.; Wen, W.; Zhao, Y.-D. Recent advances in electrochemical sensing for hydrogen peroxide: a review. *Analyst* **2012**, *137*, 49-58.
(21) Roberts, J. G.; Voinov, M. A.; Schmidt, A. C.; Smirnova, T.; Sombers, L. A. The Hydroxyl Radical is a Critical Intermediate in the Voltammetric Detection of Hydrogen Peroxide. *J. Am. Chem. Soc.* **2016**, *138*, 2516−2519.
(22) Jirkovský, J. S.; Panas, Itai; Ahlberg, E.; Halasa, M.; Romani, S.; Schiffrin, D. J. Single Atom Hot-Spots at Au–Pd Nanoalloys for Electrocatalytic H_2O_2 Production. *J. Am. Chem. Soc.* **2011**, *133*, 19432–19441.
(23) Siahrostami, S.; Verdaguer-Casadevall, A.; Karamad, M.; Deiana, D.; Malacrida, P.; Wickman, B.; Escudero-Escribano, M.; Paoli, E. A.; Frydendal, R.; Hansen, T. W.; Chorkendorff, I.; Stephens, I. E. L.; Rossmeisl, J. Enabling direct H_2O_2 production through rational electrocatalyst design. *Nature Mater.* **2013**, *12*, 1137–1143.
(24) Sa, Y. J.; Kim, J. H.; Joo, S. H. Active Edge-Site-Rich Carbon Nanocatalysts with Enhanced Electron Transfer for Efficient Electrochemical Hydrogen Peroxide Production. *Angew. Chem. Int. Ed.* **2019**, *58*, 1100-1105.
(25) Wang, Y.; Noel, J.-M.; Velmurugan, J.; Nogala, W.; Mirkin, M. V.; Lu, C.; Guille Collignon, M.; Lemaître, F.; Amatore, C. Nanoelectrodes for Determination of Reactive Oxygen and Nitrogen Species Inside Murine Macrophages. *Proc. Natl. Acad. Sci. USA* **2012**, *109*, 11534-11539.
(26) van Stroe-Biezen, S. A. M.; Everaerts, F. M.; Janssen, L. J. J.; Tacken, R. A. Diffusion coefficients of oxygen, hydrogen peroxide and glucose in a hydrogel. *Anal. Chim. Acta* **1993**, *273*, 553-560.
(27) Li, Y.; Hu, K.; Yu, Y.; Rotenberg, S. A.; Amatore, C.; Mirkin, M. V. Direct Electrochemical Measurements of Reactive Oxygen and Nitrogen Species in Nontransformed and Metastatic Human Breast Cells. *J. Am. Chem. Soc.* **2017**, *139*, 13055−13062.
(28) Shim, J. H.; Kim, J.; Lee, C.; Lee, Y. Electrocatalytic Activity of Gold and Gold Nanoparticles Improved by Electrochemical Pretreatment. *J. Phys. Chem. C* **2011**, *115*, 305–309.
(29) Xu, K.; Zhao, J.; Moore, E. G. Photo-Induced Electron Transfer in a Diamino-Substituted $Ru(bpy)_3[PF_6]_2$ Complex and Its Application as a Triplet Photosensitizer for Nitric Oxide (NO)-Activated Triplet-Triplet Annihilation Upconversion. *Photochem. Photobiol. Sci.* **2016**, 15, 995−1005.
(30) Li, X.; Majdi, S.; Dunevall, J.; Fathali, H.; Ewing, A. G. Quantitative measurement of transmitters in individual vesicles in the cytoplasm of single cells with nanotip electrodes. *Angew. Chem. Int. Ed.* **2015,** *54*, 11978-11982.
(31) Li, Y.-T.; Zhang, S.-H.; Wang, X.-Y.; Zhang, X.-W.; Oleinick, A. I.; Svir, I.; Amatore, C.; Huang, W.-H. Real-time monitoring of discrete synaptic release events and excitatory potentials within self-reconstructed neuro-muscular junctions. *Angew. Chem. Int. Ed.* **2015**, *54*, 9313-9318.
(32) Rees, H. R.; Anderson, S. E.; Privman, E.; Bau, H. H.; Venton B. J. Carbon Nanopipette Electrodes for Dopamine Detection in Drosophila. *Anal. Chem.* **2015**, *87*, 3849−3855.
(33) Pan, R.; Hu, K.; Jiang, D.; Samuni, U.; Mirkin, M. V. Electrochemical Resistive-Pulse Sensing. *J. Am. Chem. Soc.* **2019**, *141*, 19555-19559.
(34) Jalkh, J.; Leroux, Y.; Vacher, A.; Lorcy, D.; Hapiot, P.; Lagrost, C. Tetrathiafulvalene-Tetracyanoquinodimethane Charge-Transfer Complexes Wired to Carbon Surfaces: Tuning of the Degree of Charge Transfer. *J. Phys. Chem. C* **2016**, *120*, 28021–28030.

For TOC only

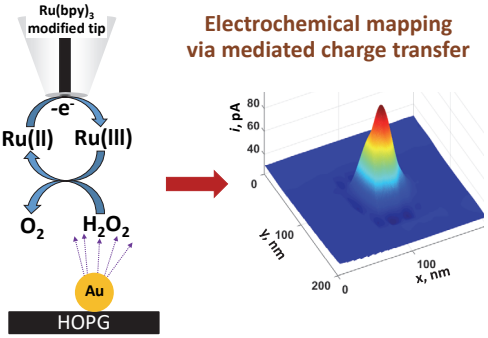
Ru(bpy)3
modified tip
-e-
Ru(II)
Ru(III)
O2
H2O2
Au
HOPG
Electrochemical mapping
via mediated charge transfer
i, pA
80
60
40
0
y, nm
100
200
0
100
x, nm